MASTER

Electrical stimulation of bone growth calculation of the electromagnetic field distribution in a thigh

van Amelsfort, A.M.J.

Award date:
1983

ELECTRICAL STIMULATION OF BONE GROWTH
CALCULATION OF THE ELECTROMAGNETIC FIELD DISTRIBUTION IN A THIGH

by A.M.J. van Amelsfort

ET-11-83

This study is performed in partial fulfilment of the requirements of the degree of Master of Science(ir) at the Eindhoven University of Technology under the supervision of

prof.dr.ir. J.E.W. Beneken
ir. Th. Scharten
drs. J.M.M. Roelofs

Eindhoven, June 1983.

ABSTRACT

To date, in studies about electrically stimulated osteogenesis, the electromagnetic field distribution in the vicinity of the individual bone cell has only been a matter of speculation. In the present study a model is developed to calculate the field within a limb (e.g.,a thigh) for an arbitrary electromagnetic source distribution. For this purpose the thigh is modelled as a composite circular cylindrical electrical waveguide with infinite length; each layer represents a different biological tissue. The electrical properties are assumed to be linear, reciprocal, homogeneous but anisotropic with respect to the axial direction (z axis). Thus, the active boundary value field problem can be reduced to an algorithm leading to an analytical formulation of Green functions for an arbitrary number of layers and arbitrary source distributions.

The algorithm was tested for a system consisting of a circular, cylindrical anisotropic bone surrounded by lossy air and a homogeneously charged ring inside the bone, and for a system where bone was replaced by an isotropic insulator. The test results show the axial and radial electric field distribution as a function of axial and radial coordinates.

Janssen [8] studied electrical stimulation of bone growth in the vicinity of two ring shaped electrodes placed on an intramedullary rod. With the computer model the electric field distribution was reconstructed for this particular electrode arrangement, with bone and air, and a source frequency of 1 Hz. These simulation tests lead to the following conclusions: firstly, anisotropy greatly influences the electric field distribution for source frequencies near the transverse relaxation frequency; secondly, the field within the bone tissue is almost parallel to the z axis; just outside the bone the field has a different orientation; thirdly, the electrodes do not only induce a

charge distribution in the vicinity of the electrodes (electrochemical double layer) but also a surface charge distribution at the bone/air boundary.

The computer programs have a large dynamic range for the different parameters (source frequencies from 1Hz to 1MHz, real part of the permittivity from ε_0 to $10^4 \cdot \varepsilon_0$, conductivity from 0 to 10^{-2} $\Omega^{-1}m^{-1}$). The computer programs permit the calculation of the electromagnetic field distribution for systems consisting of bone and additional tissues like marrow, muscle and fat, and for arbitrary stimuli like electrodes or coils.

LIST OF PRICIPLE SYMBOLS.

$\underline{a}$	unit vector
$\underline{E}$	electric field phasor
f	frequency
$\underline{H}$	magnetic field phasor
$\underline{J}$	primary electric current density
$\underline{K}$	primary magnetic current density
$\underline{n}$	unit vector along normal
r	radius, radial coordinate
t	time coordinate
β	spatial frequency, axial phase factor
δ	impulse function
$\underline{\underline{\varepsilon}}$	complex tensor permittivity
ϕ	azimuthal coordinate
κ	transverse wave number
$\underline{\underline{\mu}}$	complex tensor permeability
ρ	primary electric charge density
$\underline{\underline{\sigma}}$	tensor conductivity
ω	radian frequency
∇	del operator
∂_j	partial derivation with respect to some coordinate j

The following superscripts are used

e	electric component
h	magnetic component

as subscripts

i	number of the layer
J	Bessel component
o	observation
s	source
t	transverse component
Y	Neumann component
z	axial component
τ	transverse tangential component
ν	transverse normal component

CONTENTS.

1. INTRODUCTION

Eversince the discovery of 'electricity', men has tried to use it clinically, for diagnostic as well as therapeutic purposes. With the help of sophisticated electronic devices, it is now possible to obtain all sorts of information about a patient through electric measurements. The electro cardio gram is probably the best known example. In the past many attempts have been made to find therapeutic applications of electricity [7], but only few standard therapies have been developed; the pace-maker for the heart is an example that is widely used.

Another area, attracting a lot of scientific attention, is the use of electricity in osteogenesis. Although, many experiments have been done, only since the discovery of the piezoelectric property of bone, found by Yasuda in 1953[16], the clinical interest increased rapidly. Because electricity, or better, electro-magnetism, can appear in many different forms, different methods have been used to stimulate osteogenesis, with different results [13]. Perhaps this is a reason, that different models have been made to explain the observed phenomena. These models however, result in 'more questions than answers' [2]. One of these questions is about the electrical stimulus itself. Little is known about the properties of the electromagnetic field in the vicinity of the stimulated area, induced by a stimulator or by the biological tissues themselves.

In this report a model will be developed, by which it is possible to compute, in first order of approximation, the local electromagnetic field in an intact thigh, for an arbitrary distribution of the electro-magnetic sources. After introducing the model used, a description of the

problem will be given in Section 2. In Section 3 a theoretical analysis of the boundary value problem, an algorithm to compute the numerical value of the solution and an interpretation of the resulting formulae will be given, respectively. Furthermore in Section 4 numerical results are given and the discussion follows in Section 5. Finally, a clinical illustration is given in Section 6. For more details about the derivation and the computer programs, the reader is referred to appendices A and B.

Although the aim of this investigation is to calculate the electromagnetic field in a bone, the results can also be applied in other areas of guided wave propagation. In communication systems, where waveguides are used (optical fiber), the proposed method could be used to find an analytical solution of active field problems for isotropic or anisotropic media.

2. STATEMENT OF THE PROBLEM

As mentioned in the introduction, the behaviour of the electromagnetic field must be known in the vicinity of an individual bone cell, in order to explain the observed phenomena occuring during electrical stimulated osteogenesis. Although the human skeleton consists of many different bones, with various structures and functions, in this report the attention is only focussed upon the femur and it's surroundings (upperleg). In Fig.2.1 a schematic drawing of a thigh is shown. Because this system is very complicated, some approximations are made on geometry and electrical properties of the tissues. For a detailed biological discription the reader is referred to [15].

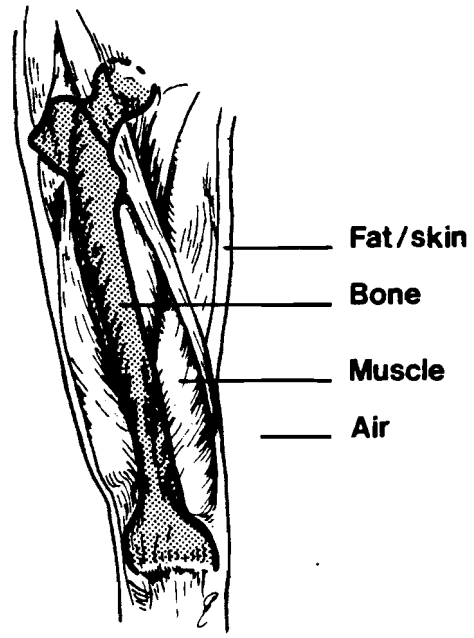

Fig.2.1 Schematic drawing of an upperleg.

With respect to geometry, it is assumed that

-the transition of one tissue to another is abrupt;

-the tissues form concentric circular cylindrical layers;

-the structure is of infinite length.

A picture of this model is shown in Fig.2.2 .

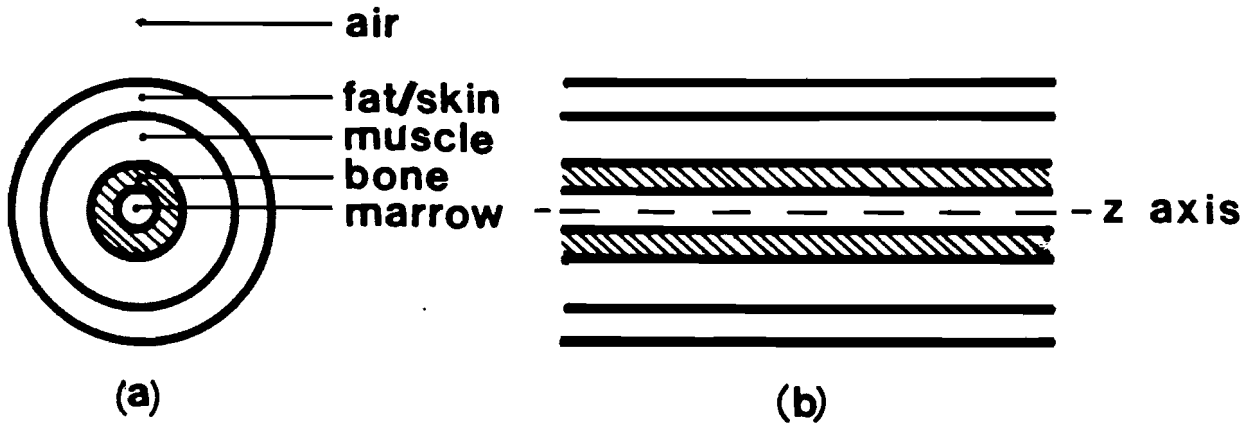

Fig.2.2 Schematic drawing of the model(femur system);
(a) cross section, (b) longitudinal section.

Secondly, the electrical properties of the tissues involved are assumed to be as follows

-time independent;

-linear;

-reciprocal;

-homogeneous;

-anisotropic, with respect to the axial direction.

Finally, something has to be said about the electromagnetic sources involved. There are natural and artificial electromagnetic sources.

One of the natural sources is the piezoelectric property of bone. Secondly the periosteum and the endosteum act as semi-permeable layers. A concentration gradient of ions across each layer is the result. Furthermore the metabolic activity in an organ results in a net negative free charge. The epiphysial discs, being more active than the diaphysial region, result in a concentration gradient of free charge within the femur. Although the list is not complete, a last kind of natural sources to be mentioned here, are the streaming potentials, caused by the streaming of charged particles in fluids like blood.

The artificial sources can be devided into two subclasses, depending on the nature of the stimulator used (electrodes [8] or coils [1]). Although a great variety of stimulators are being used [13], these can all be described in terms of primary electric and/or magnetic current distributions.

As will be clear from the above catalogue, for the present no electromagnetic source can be excluded, to calculate the field in a femur system. So, the problem is to find the field in a femur system excited by an arbitrary configuration of electromagnetic sources. More precisely, the solution has to be found to Maxwell's inhomogeneous differential equations. In the frequency domain, these equations read

$$\nabla \times \underline{E} + j\omega \underline{\underline{\mu}} \cdot \underline{H} = -\underline{K} \tag{2.1}$$

$$\nabla \times \underline{H} - j\omega \underline{\underline{\varepsilon}} \cdot \underline{E} = \underline{J} \tag{2.2}$$

where

$\underline{E}$ is the electric field phasor,
$\underline{H}$ is the magnetic field phasor,
$\underline{J}$ is the primary electric current density,
$\underline{K}$ is the primary magnetic current density,
$\underline{\underline{\mu}}$ is the tensor permeability ,
$\underline{\underline{\varepsilon}}$ is the tensor permittivity .

The electric and magnetic field phasors satisfy the boundary conditions

$\underline{n} \times \underline{E}$ being continuous across a boundary surface, (2.3)

$\underline{n} \times \underline{H}$ being continuous across a boundary surface, (2.4)

the solution must describe a field with finite energy. (2.5)

The time dependency of the field components is found by inverse transformation according to

$$F =: \frac{1}{2\pi} \int_{-\infty}^{\infty} F \exp(j\omega t) d\omega \qquad (2.6)$$

As the system is linear, the responses to the primary electric or magnetic currents can be examined separately. In this report only the response to the electric current distribution will be derived, so $\underline{K}=\underline{0}$. With the use of two transformations, the three dimensional problem will be changed into a one dimensional problem. The axial dependency (z) is transformed to the spatial frequency domain (β),using a Fourier transform, according to

$$F =: \int_{-\infty}^{\infty} F \exp(-j\beta z)dz. \tag{2.7}$$

The azimuthal dependency (ϕ) is transformed by a finite Fourier integral

$$F =: \int_{-\pi}^{\pi} F \exp(-jn\phi)d\phi \tag{2.8}$$

To derive the field exprssions,

- -the transverse vector components of the electric and magnetic field phasors will be written in terms of the axial field components;
- -the boundary value problem for the axial field components will be solved for a source distribution on a cylindrical surface of arbitrary radius; the solution is the transformed Green function for the axial field components;
- -the transformed Green function will be inverted back to the axial domain.

Finally, the result will be the time harmonic field solution for a given source distribution at a given source frequency.

3. ANALYSIS

In electromagnetic terms the femur system can be described as an (infinitely long) anisotropic, composite circular cylindrical waveguide. The theory of guided electro-magnetic waves can in priciple be applied [6],[11]. However, this theory is commonly used for isotropic materials. This means that it cannot directly be used for the femur system. In the following, this theory is extended to anisotropic media.

3.1 Boundary value problem

Field equations

Separating the axial and the transverse vector components,

$$\underline{E} = \underline{E}_t + E_z \underline{a}_z \qquad (3.1a)$$

$$\underline{H} = \underline{H}_t + H_z \underline{a}_z \qquad (3.1b)$$

$$\nabla = \nabla_t + \underline{a}_z \partial_z \qquad (3.1c)$$

$$\underline{J} = \underline{J}_t + J_z \underline{a}_z \qquad (3.1d)$$

$$\underline{K} = \underline{K}_t + K_z \underline{a}_z \qquad (3.1e)$$

$$\nabla_t = (\partial_x, \partial_y, 0) \qquad (3.1f)$$

and defining the tensor permittivity and tensor permeability as

$$\underline{\underline{\varepsilon}} = \begin{bmatrix} \varepsilon_t & 0 & 0 \\ 0 & \varepsilon_t & 0 \\ 0 & 0 & \varepsilon_z \end{bmatrix} \quad (3.2a), \qquad \underline{\underline{\mu}} = \begin{bmatrix} \mu_t & 0 & 0 \\ 0 & \mu_t & 0 \\ 0 & 0 & \mu_z \end{bmatrix} \quad (3.2b),$$

eqns.(2.1) and (2.2) change into

$$\nabla_t \times \underline{E}_t + j\omega\mu_z H_z \underline{a}_z = -K_z \underline{a}_z \tag{3.3a}$$

$$\nabla_t \times \underline{H}_t - j\omega\varepsilon_z E_z \underline{a}_z = J_z \underline{a}_z \tag{3.3b}$$

$$\underline{a}_z \times \partial_z \underline{E}_t + \nabla_t \times \underline{a}_z E_z + j\omega\mu_t \underline{H}_t = -\underline{K}_t \tag{3.3c}$$

$$\underline{a}_z \times \partial_z \underline{H}_t + \nabla_t \times \underline{a}_z H_z - j\omega\varepsilon_t \underline{E}_t = \underline{J}_t \tag{3.3d}$$

Because only linear media are considered, the responses to the various sources can be examined separately, and summed afterwards. The derivation, being straightforward for each source type, will be given only for the electric current density .

Using the Fourier transformation (eqn.(2.7)) the field equations are written as

$$\nabla_t \times \underline{E}_t + j\omega\mu_z H_z \underline{a}_z = \underline{0} \tag{3.4a}$$

$$\nabla_t \times \underline{H}_t - j\omega\varepsilon_z E_z \underline{a}_z = J_z \underline{a}_z \tag{3.4b}$$

$$j\beta\, \underline{a}_z \times \underline{E}_t + \nabla_t \times \underline{a}_z E_z + j\omega\mu_t \underline{H}_t = \underline{0} \tag{3.4c}$$

$$j\beta\, \underline{a}_z \times \underline{H}_t + \nabla_t \times \underline{a}_z H_z - j\omega\varepsilon_t \underline{E}_t = \underline{J}_t \tag{3.4d}$$

In order to write $\underline{E}_t$, $\underline{H}_t$ as an explicit function of E_z and H_z, $\underline{H}_t$ is eliminated from eqns.(3.4c) and (3.4d) and $\underline{E}_t$ is eliminated in a simular way.
The result is then given by

$$\underline{E}_t = \kappa^{-2} \left(j\beta\, \nabla_t E_z + j\omega\mu_t \underline{a}_z \times \nabla_t H_z + j\omega\mu_t \underline{J}_t \right) \tag{3.5a}$$

$$\underline{H}_t = \kappa^{-2} \left(j\beta \nabla_t H_z - j\omega\varepsilon_t \underline{a}_z \times \nabla_t E_z - j\beta \underline{a}_z \times \underline{J}_t \right) \tag{3.5b}$$

where,

$$\kappa^2 = -\beta^2 + \omega^2 \varepsilon_t \mu_t \tag{3.6a}$$

To find the differential equations for the functions E_z and H_z , $\nabla_t \times \underline{H}_t$ in eqn.(3.4b) is eliminated by taking the transverse curl of eqn. (3.4c) using the vector identity,

$$\nabla_t \times (\underline{a}_z \times \underline{v}) = \underline{a}_z \, (\nabla_t \cdot \underline{v}) \tag{3.7}$$

and then eliminating $\nabla_t \cdot \underline{E}_t$ by taking the transverse divergence of eqn.(3.4d). For H_z an analogous procedure can be followed. The differential equations are found to be

$$\nabla_t^2 E_z + (\kappa^e)^2 E_z = \left(\frac{\beta^2}{j\omega\varepsilon_t} + j\omega\mu_t \right) J_z - \frac{j\beta}{j\omega\varepsilon_t} \nabla_t \cdot \underline{J}_t \tag{3.8a}$$

$$\nabla_t^2 H_z + (\kappa^h)^2 H_z = -\underline{a}_z \cdot (\nabla_t \times \underline{J}_t) \tag{3.8b}$$

where

$$(\kappa^e)^2 = -\frac{\varepsilon_z}{\varepsilon_t} \beta^2 + \omega^2 \varepsilon_z \mu_t \tag{3.6b}$$

$$(\kappa^h)^2 = -\frac{\mu_z}{\mu_t} \beta^2 + \omega^2 \varepsilon_t \mu_z . \tag{3.6c}$$

The definition of three different transverse wavenumbers (κ) is a consequence of the anisotropic property of the materials. When the media are isotropic, $\varepsilon_z=\varepsilon_t$ and $\mu_z=\mu_t$, the wavenumbers are identical, which is in agreement with other literature [6], [11].

Because in this report, as an example, only the response of the system to electric charge has been calculated, in the following, the current supplying the charge is neglected. Thus

$$-\underline{a}_z \cdot (\nabla_t \times \underline{J}_t)$$

and

$$j\omega\mu_t J_z$$

are taken as zero and

$$\frac{j\beta}{j\omega\varepsilon_t}\left(j\beta J_z + \nabla_t \cdot \underline{J}_t\right) = \frac{j\beta}{j\omega\varepsilon_t}\nabla\cdot\underline{J} = -\frac{j\beta}{\varepsilon_t}\rho \qquad (3.9)$$

ρ being the free electric charge density.

Boundary equations [12]

The solution of the differential equations (eqns.(3.8)) must answer the boundary conditions formulated by eqns.(2.3), (2.4) and (2.5). It can be shown [12] that for each boundary surface the first two conditions change in

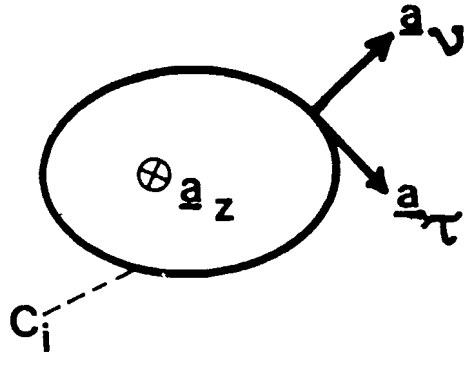

$$E_z^- = E_z^+ \qquad r \in C_i \qquad (3.10a)$$

$$(\kappa^-)^{-2}(j\beta\, \partial_\tau E_z^- + j\omega\mu_t^-\, \partial_\nu H_z^-) =$$

$$(\kappa^+)^{-2}(j\beta\, \partial_\tau E_z^+ + j\omega\mu_t^+ \partial_\nu H_z^+) \quad ,r \in C_i \qquad (3.10b)$$

$$H_z^- = H_z^+ \qquad ,r \in C_i \qquad (3.10c)$$

$$(\kappa^-)^{-2}(j\beta\, \partial_\tau H_z^- - j\omega\varepsilon_t^-\, \partial_\nu E_z^-) =$$

$$(\kappa^+)^{-2}(j\beta\, \partial_\tau H_z^+ - j\omega\varepsilon_t^+ \partial_\nu E_z^+) \quad ,r \in C_i \qquad (3.10d)$$

where ∂_τ, ∂_ν are the partial derivates with respect to the tangential and normal directions off the surface respectively. The superscripts (+/-) are used to indicate the exterior and interior fields.

When the electric charge is concentrated on a uniform sheet, eqns.(3.8) imply the following boundary conditions, to be fullfilled at the source boundary

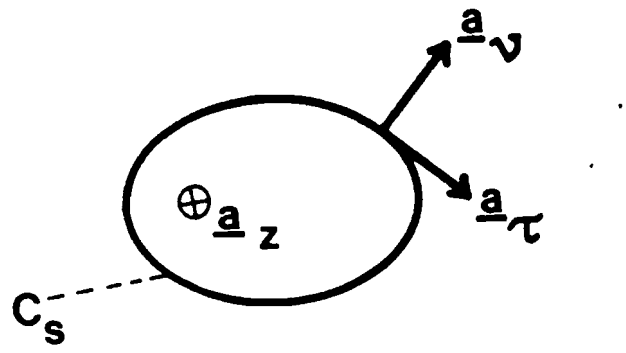

$$E_z^+ - E_z^- = 0 \qquad ,r \in C_s \qquad (3.11a)$$

$$\partial_\nu E_z^+ - \partial_\nu E_z^- = \frac{j\beta}{\varepsilon_t} \rho \qquad ,r \in C_s \qquad (3.11b)$$

$$H_z^+ - H_z^- = 0 \qquad ,r \in C_s \qquad (3.11c)$$

$$\partial_\nu H_z^+ - \partial_\nu H_z^- = 0 \qquad ,r \in C_s \qquad (3.11d)$$

where ρ is now representing the surface charge density.

Boundary value problem in cylindrical coordinates

Because the theory must be applied to a circular symetric system, the coordinates are transformed to a circular cylindrical configuration, the transverse del operator ∇_t is written as

$$\nabla_t = \underline{a}_r \partial_r + \underline{a}_\phi jnr^{-1} \qquad (3.12)$$

and

$$\nabla_t^2 = r^{-1}\partial_r(r\ \partial_r) - n^2 r^{-2} \qquad (3.13)$$

Using eqns.(3.12) and (3.13) and substitution of eqn.(3.9) into eqns. (3.8) gives

$$\frac{1}{r}\partial_r(\ r\ \partial_r E_z\ ) + \left[(\kappa^e)^2 - \frac{n^2}{r^2}\right] E_z = \frac{j\beta\rho}{\varepsilon_t} \qquad (3.14a)$$

$$\frac{1}{r}\partial_r(\ r\ \partial_r H_z\ ) + \left[(\kappa^h)^2 - \frac{n^2}{r^2}\right] H_z = 0 \qquad (3.14b)$$

These two equations are Bessel differential equations, both of the order n with different wavenumbers.

The boundary conditions (eqns(3.11)) at the source boundary can now be written as

$$E_z^+ - E_z^- = 0 \qquad , r = r_s \qquad (3.17a)$$

$$\partial_r E_z^+ - \partial_r E_z^- = \frac{j\beta\rho(n,\beta,\omega)}{r'\epsilon_t} \qquad , r = r_s \qquad (3.17b)$$

$$H_z^+ - H_z^- = 0 \qquad , r = r_s \qquad (3.17c)$$

$$\partial_r H_z^+ - \partial_r H_z^- = 0 \qquad , r = r_s \qquad (3.17d)$$

and for the other boundaries (eqns. (3.10))

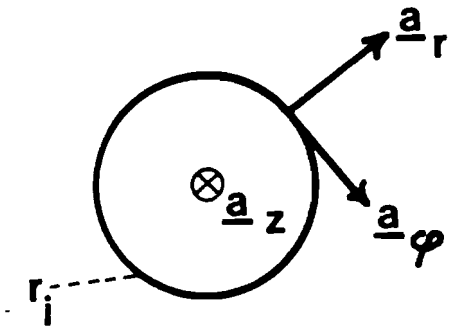

$$E_z^- = E_z^+ \qquad , r = r_i \qquad (3.18a)$$

$$\kappa^{+2}(j\beta \frac{jn}{r} E_z^- + j\omega\mu_t^- \partial_r H_z^-) = \kappa^{-2}(j\beta \frac{jn}{r} E_z^+ + j\omega\mu_t^+ \partial_r H_z^+), \; r = r_i \qquad (3.18b)$$

$$H_z^- = H_z^+ \qquad , r = r_i \qquad (3.18c)$$

$$\kappa^{+2}(j\beta \frac{jn}{r} H_z^- - j\omega\varepsilon_t^- \partial_r E_z^-) = \kappa^{-2}(j\beta \frac{jn}{r} H_z^+ - j\omega\varepsilon_t^+ \partial_r E_z^+), \; r = r_i \qquad (3.18d)$$

As can be observed, for non circular symetric configurations ($n \neq 0$), the axial field components are mutual dependent through the boundary conditions.

In each area, the general solution of the homogeneous Bessel differential equations of integer order can be formed by a lineair combination of Bessel and Neumann functions

$$E_{z,i}(r) = C^e_{J,i} J_n(\kappa^e_i r) + C^e_{Y,i} Y_n(\kappa^e_i r) \qquad (3.19a)$$

$$H_{z,i}(r) = C^h_{J,i} J_n(\kappa^h_i r) + C^h_{Y,i} Y_n(\kappa^h_i r) \qquad (3.19b)$$

where subscript i indicates the number of the layer. For each layer four amplitude constants can be found by applying the boundary conditions to the general solution (eqns.(3.19)). Furthermore, the solution describing a field with finite energy (eqn.(2.5)) leads to 4 additional conditions. At r=0 the Neumann functions are singular so, for the central region these functions do not contribute to the solution

$$C^e_{Y,1} = 0 \qquad (3.20)$$

$$C^h_{Y,1} = 0 \qquad (3.21)$$

Furthermore as $r \to \infty$ the solution must be a Hankel-function of the second kind this implies

$$C^{e}_{Y,N} = -j\, C^{e}_{J,N} \tag{3.22}$$

$$C^{h}_{Y,N} = -j\, C^{h}_{J,N} \tag{3.23}$$

where N indicates the exterior region. Once the coefficients are determined the Green function is found for a source distribution in one layer.

3.2 Algorithm

In this paragraph an algorithm will be derived, to find the transformed Green function for an arbitrary number of layers and an arbitrary location of the source. For more details the reader is referred to appendix B.

First the layers and boundaries are renumbered to include the extra

boundary conditions at $r=r_s$. The layer containing the source is split up and the numbering for the layers and the boundaries starts with 1 for the central region and then increments to the exterior region. As an example see Fig.3.1.

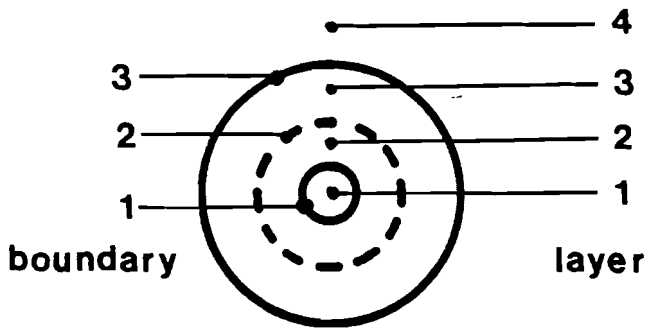

Fig.3.1 Renumbering of the layers and boundaries.

Now there are $4\times(N+1)$ coefficients to determine, by as many boundary conditions. We have N boundaries with 4 conditions for each boundary (eqns.(3.17) and (3.18)) and 4 additionally conditions formed by eqns.(3.20) trough (3.23). Using linear algebra, the boundary conditions can be written as

$$\underline{\underline{A}}_i \cdot \underline{C}_i = \underline{\underline{B}}_i \cdot \underline{C}_{i+1} \qquad r = r_i \ , \ r \neq r_s \qquad (3.24)$$

$$\underline{C}_i = \underline{C}_{i+1} + \underline{\underline{D}} \cdot \underline{S} \qquad r = r_s \qquad (3.25)$$

where,

$$\underline{C}_i = (C^e_{J,i}, C^e_{Y,i}, C^h_{J,i}, C^h_{Y,i})^T \qquad (3.26a)$$

$$\underline{C}_{i+1} = (C^{e}_{J,i+1}, C^{e}_{Y,i+1}, C^{h}_{J,i+1}, C^{h}_{Y,i+1})^{T} \tag{3.26b}$$

and

$$\underline{S} = \left(0 \, , \, 0 \, , \, -\frac{j\beta\rho}{\varepsilon_t r_s} \, , 0 \right)^{T} \tag{3.26c}$$

The above matrices are written out in full in Appendix A. The coefficients of the first layer can now be written as a function of those of the exterior region by

$$\left[\prod_{\substack{i=N \\ i \neq s}}^{1} \left(\underline{\underline{B}}_i^{-1} \cdot \underline{\underline{A}}_i \right) \right] \cdot \underline{C}_1 = \underline{C}_{N+1} + \left[\prod_{i=s+1}^{N} \left(\underline{\underline{B}}_i^{-1} \cdot \underline{\underline{A}}_i \right) \right] \cdot \underline{\underline{D}}^{-1} \cdot \underline{S} \tag{3.27}$$

Eliminating the amplitude constants of the Neumann functions by eqns.(3.20) and (3.21) and rearranging the 4 coëfficients of the Bessel functions in eqn.(3.27) gives

$$(C^{e}_{J,1}, C^{h}_{J,1}, C^{e}_{J,N+1}, C^{h}_{J,N+1})^{T} = \underline{\underline{DSP}}^{-1} \cdot \left[\prod_{i=N}^{s+1} \left(\underline{\underline{B}}_i^{-1} \cdot \underline{\underline{A}}_i \right) \right] \cdot \underline{\underline{D}}^{-1} \cdot \underline{S} \tag{3.28}$$

Finally, when the 4 coefficients of the Bessel functions are known, the other coefficients can be determined, and the transformed Green functions are found as a combination of Bessel and Neumann functions.

3.3 Transfer function

In the previous paragraph it has been shown, that in each layer the axial field components can be written as linear combinations of Bessel

and Neumann functions, and the coefficients themselves depend linearly on the source vector. Choosing a particular source radius (r_s is fixed), and a radius of observation ($r=r_o$), axial field components are given by (the subscript i is omitted)

$$E_z = C_J^e \, J_n(\kappa^e r_o) + C_Y^e \, Y_n(\kappa^e r_o) \tag{3.29a}$$

$$H_z = C_J^h \, J_n(\kappa^h r_o) + C_Y^h \, Y_n(\kappa^h r_o) \tag{3.29b}$$

In general , in each region these functions can also be written as

$$(E_z, H_z)^T = \underline{\underline{T}} \cdot \underline{S} \tag{3.30}$$

where $\underline{\underline{T}}$ can be interpreted as the transfer function of the system for this particular combination of r_s and r_o. When only free electric charge act as the source, the source vector is

$$\underline{S} = (0 , 0 , - \frac{j\beta\rho}{\varepsilon_t r_s} , 0)^T \tag{3.31}$$

and the axial electric field distribution is

$$E_z = - T_{1,3} \, (r_o, n, \beta, \omega, r_s) \, \frac{j\beta}{\varepsilon_t r_s} \, \rho \, (n, \beta, \omega). \tag{3.32a}$$

and for the magnetic field

$$H_z = - T_{2,3} \, (r_o, n, \beta, \omega, r_s) \, \frac{j\beta}{\varepsilon_t r_s} \, \rho \, (n, \beta, \omega). \tag{3.32b}$$

Inverse transformation of β by

$$E_z(z) = \frac{1}{2\pi} \int_{-\infty}^{\infty} E_z \, \exp(j\beta z) d\beta \tag{3.33}$$

gives the field in the frequency domain (ω) as a function of the axial coordinate. Using a second inverse transformation of ω by

$$E_z(z,t) = \frac{1}{2\pi} \int_{-\infty}^{\infty} E_z(z) \exp(j\omega t) d\omega \qquad (3.34)$$

gives the field as a function of both, the axial coordinate and time. When

$$\rho(r,\phi,z,t) = \frac{\delta(r-r_s)}{r} \rho(\phi) \delta(z) \delta(t) \qquad (3.35)$$

$E_z(z,t)$ can be interpreted as the impulse response of the system with respect to the axial coordinate as well as the time coordinate. When

$$\rho(r,\phi,z,t) = \frac{\delta(r-r_s)}{r} \rho(\phi) \delta(z) \exp(j\omega_0 t) \qquad (3.36)$$

$E_z(z)$ can be interpreted as the time harmonic spatial impulse response. In the latter case the transient time function is not available.

For the computation of $E_z(z)$ a Discrete Fourier algorithm is used. It can be shown [9] that, $E_z(z)$ being a band limited function of β with bandwidth β_w, the time harmonic field distribution can be reconstructed as a function of z using

$$E_z(L \cdot \Delta z) = \frac{1}{M} \sum_{k=0}^{M-1} E_z(k \cdot \Delta\beta) W_M^{-kL} \qquad 0 \leq L \leq M-1 \qquad (3.37)$$

where

$$W_M^k = \exp(- j \frac{2\pi}{M} k) \tag{3.38}$$

are M points equally spaced in angle on the unit circle in the complex plane

$$\Delta z = \frac{2\pi}{\beta_w} \tag{3.39}$$

is the sample width in the axial direction

$$\Delta\beta = \frac{\beta_w}{M} \tag{3.40}$$

is the sample width in the spatial frequency domain and M is the number of samples used. Although there are very sophisticated algorithms to compute the time harmonic field for the entire L-intervall, in this case the Goertzel algorithm is used because only the vicinity of the source is of interest (L=0 trough L=20). The choice of β_w and M depends on the character of the amplitude spectrum of $E_z(z)$. In the next Section some numerical results will be given .

4.0 NUMERICAL RESULTS

We have calculated the time-harmonic electric field streght for a simple configuration, consisting of a solid circular cylindrical bone, surrounded by lossy air. The electromagnetic field ios assumed to be excited by an annular distribution of electric charge with harmonic time dependence, located concentrically inside the bone (see Fig.4.1).

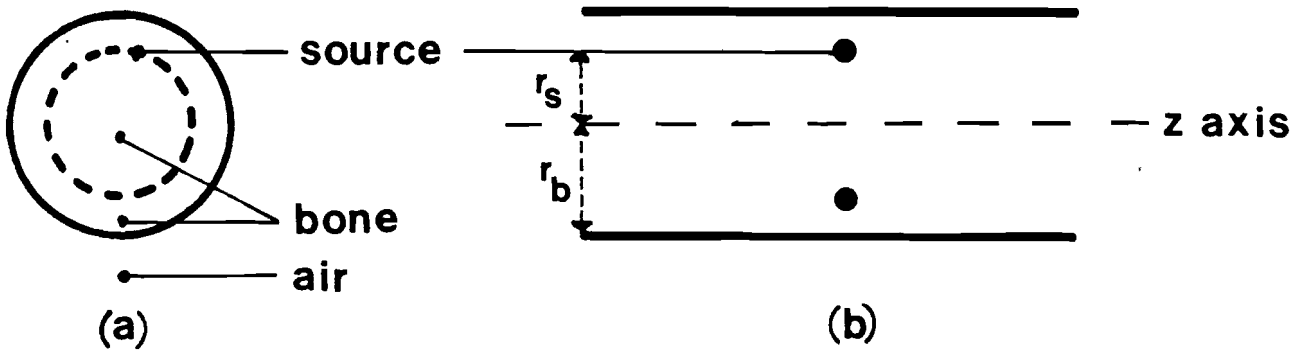

Fig.4.1 Bone configuration
(a) cross section
(b) longitudinal section.

There are two reasons for this choice. First, the simplicity of the configuration enables us to check ALTRAN procedures by deriving the equations involved by hand. Secondly, the configuration is fairly a good model for theoretically verifying some experiments, carried out at the Utrecht University Hospital [8]. A qualitative description is given in section 6. Apart from merely calculating dynamic field strengths, we wish to investigate the influence of anisotropy and disapational losses. To this end, we replace the bone by an isotropic insulator, and call this the insulator configuration. The numerical values of the electric

properties of bone are derived from Chakkalakal et. al. [4], [5]. The two configurations are given in table 4.1.

Table 4.1

central region			outer region
insulator		bone	
ε'_z	$6000\ \varepsilon_0$	$2500\ \varepsilon_0$	ε_0
ε'_t	$6000\ \varepsilon_0$	$10000\ \varepsilon_0$	ε_0
σ_z	0	$0.02\ \Omega^{-1}m^{-1}$	$10^{-6}\Omega^{-1}m^{-1}$
σ_t	0	$0.0066\ \Omega^{-1}m^{-1}$	$10^{-6}\Omega^{-1}m^{-1}$
μ	μ_0	μ_0	μ_0
$r_s = 1.0 \cdot 10^{-2}$ m			$\rho = 10^{-12}$ Cm^{-1}
$r_b = 1.5 \cdot 10^{-2}$ m			$\varepsilon = \varepsilon' - \frac{\sigma}{j\omega}$

As to source frequencies, it is supposed that the free space wavelength is very large compared with the circumference of the source. The charge distribution will then be homogeneous. This implies

$$f_s < \frac{c_0}{2\pi r_s} \approx 5000 \text{ MHz}$$

where c_0 is the plane wave velocity in free space, r_s being specified in Table 4.1. Calculations have been performed for source frequences 1 Hz $\leq f_s \leq$ 1 MHz. Because the charge is homogeneously distributed around the ring, only the first component of the Fourier-series is non-zero(n=0), the other components being zero. Therefore the azimuthal (ϕ) electric field component and the axial magnetic field component are zero, the radial electric field component is depending on the axial electric field only.

$$E_r = \kappa^{-2} j\beta \, \partial_r E_z. \tag{4.1}$$

In the following the time harmonic radial electic field component will be computed in a simular manner as the axial field.

First the amplitude spectra of the two field components for both configurations have been computed as a function of β. The spectra have been computed for two different radial distances. Furthermore in the plots, shown in Fig.4.2, the source frequency (f_s) has been used as a parameter.

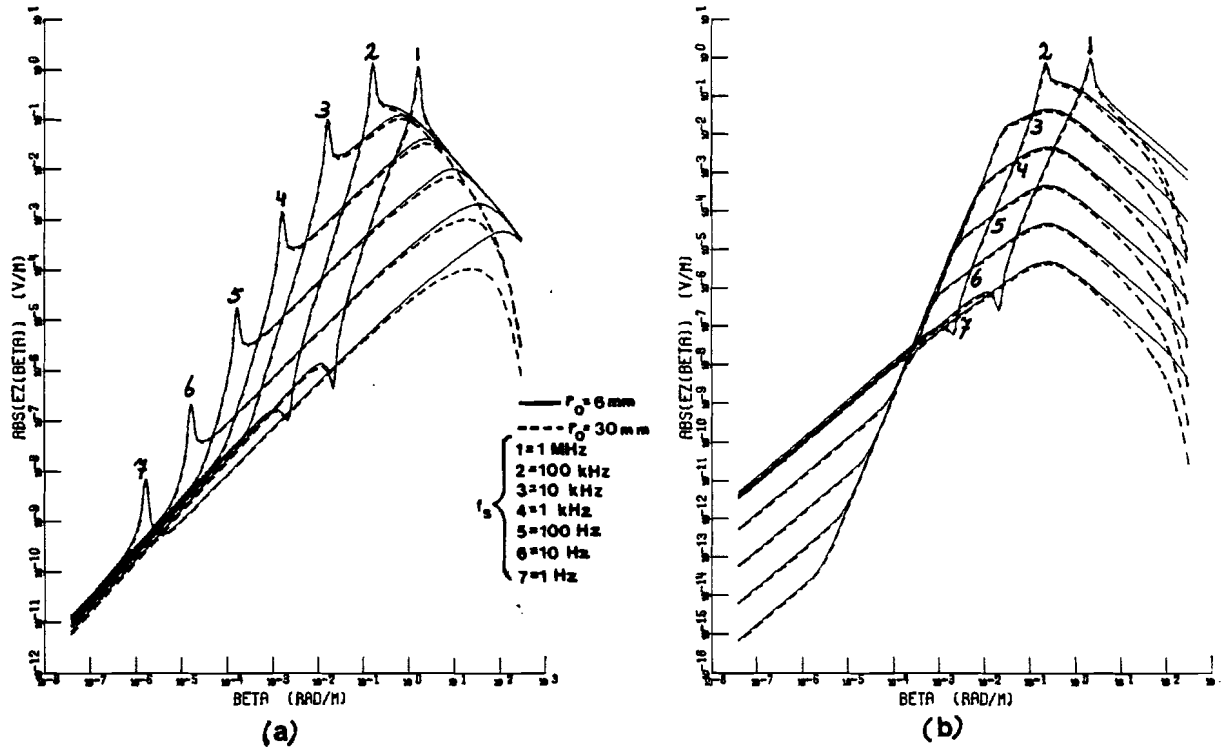

Fig.4.2 Amplitude spectrum of the axial field compnent (E_z) for both configurations at two different radial distances excited at various source frequences; (a) insulator, (b) bone.

The amplitudo spectra for both configurations show, for f_s > 100 kHz a maximum for

$$\beta_{ma}^2 = \omega^2 \varepsilon'_{t,1} \mu_0 \tag{4.2}$$

and a minimum for

$$\beta_{mi}^2 = \omega^2 \varepsilon'_{t,2} \mu_0 \tag{4.3}$$

For source frequences f_s < 10 KHz this maximum changes into a local maximum for the insulator configuration and is not observed for the bone

configuration. The local minima are not present for the lower source frequences. The spectra for the inner and outer regions show large differences for $\beta > \beta_{ma}$, only.

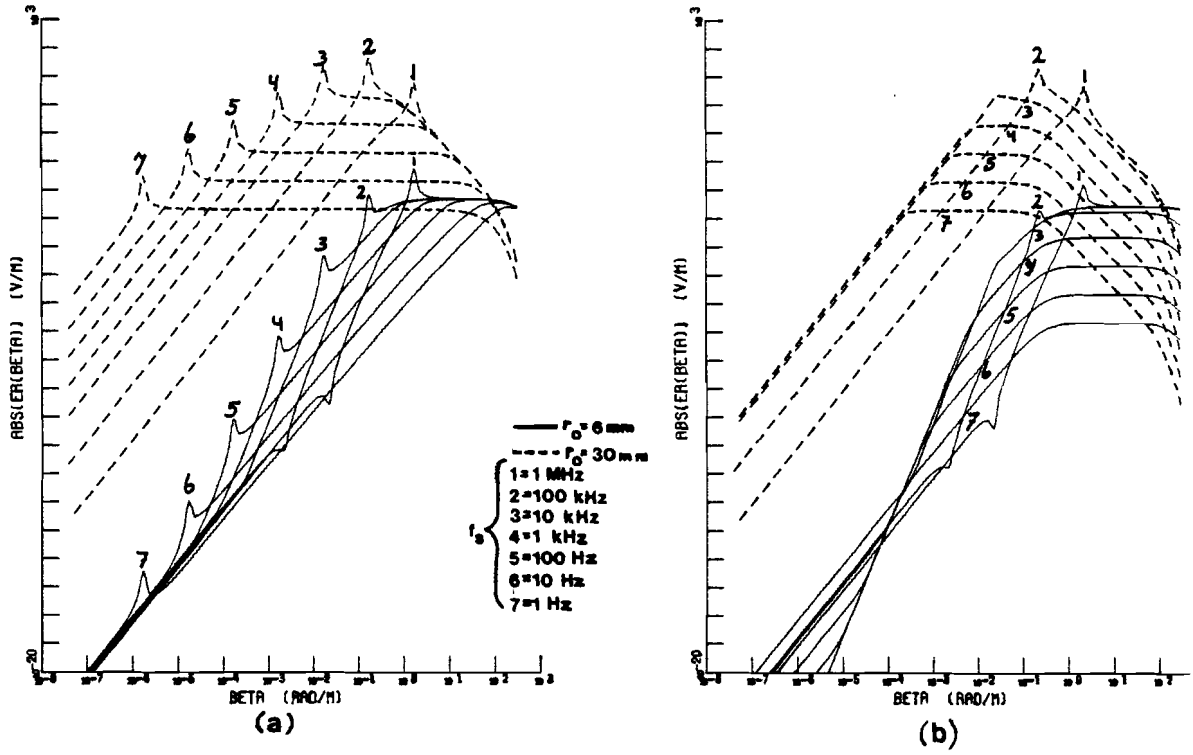

Fig.4.3 Amplitude spectrum fo the radial field component (E_r) for both configurations, at two radial distances excited at various source frequences; (a) insulator, (b) bone.

Figure 4.3 reveals the amplitude spectra of E_r for both configurations at two different radial distances. Besides the observations made for the axial field component, some characteristic differences can be seen. Comparing the spectra for the interior and exterior regions of each configuration, they show that, for the exterior region the amplitude as well as the spatial bandwidth are larger and the center spatial

frequency is shifted. Furthermore, the minimum ($\beta=\beta_{mi}$) cannot be observed in the spectra for the exterior region.

Using the Göertzel algorithm with the parameters β_w= 50 rad/m and M=300, the field components are found as a function of the axial coordinate.

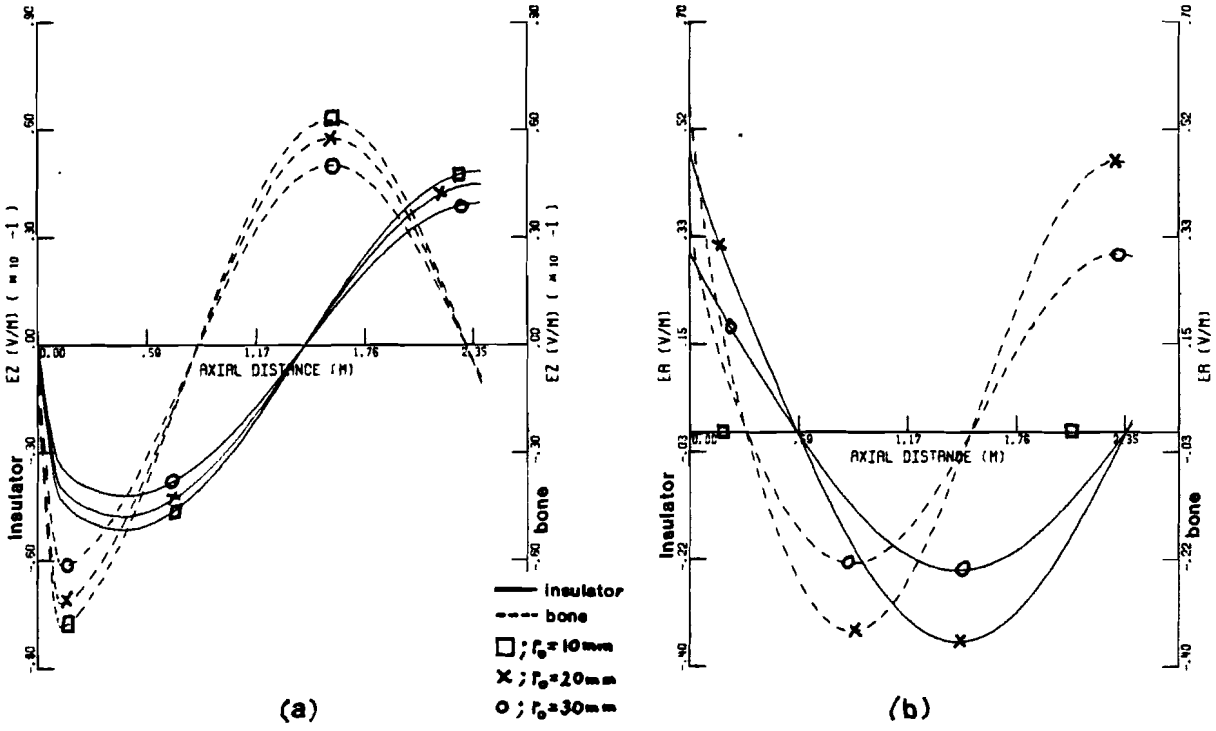

Fig.4.4 Field distributions for both configurations as a function of the axial coordinate at various radial distances. The source frequency is f_s 1 MHz; (a) axial field (E_z), (b) radial field (E_r).

Figure 4.4 shows these functions for different radial distances and a source frequency f_s=1 MHz. Apart from spatial initial effects the field components exhibit a wave distribution parallel to the z axis. The phase shift between the two field components is about $\pi/2$ radians. Interchanging the roles between the axial and radial coordinates, in Fig.4.5 the field distributions are shown as a function of the radial

distance in various transverse planes.

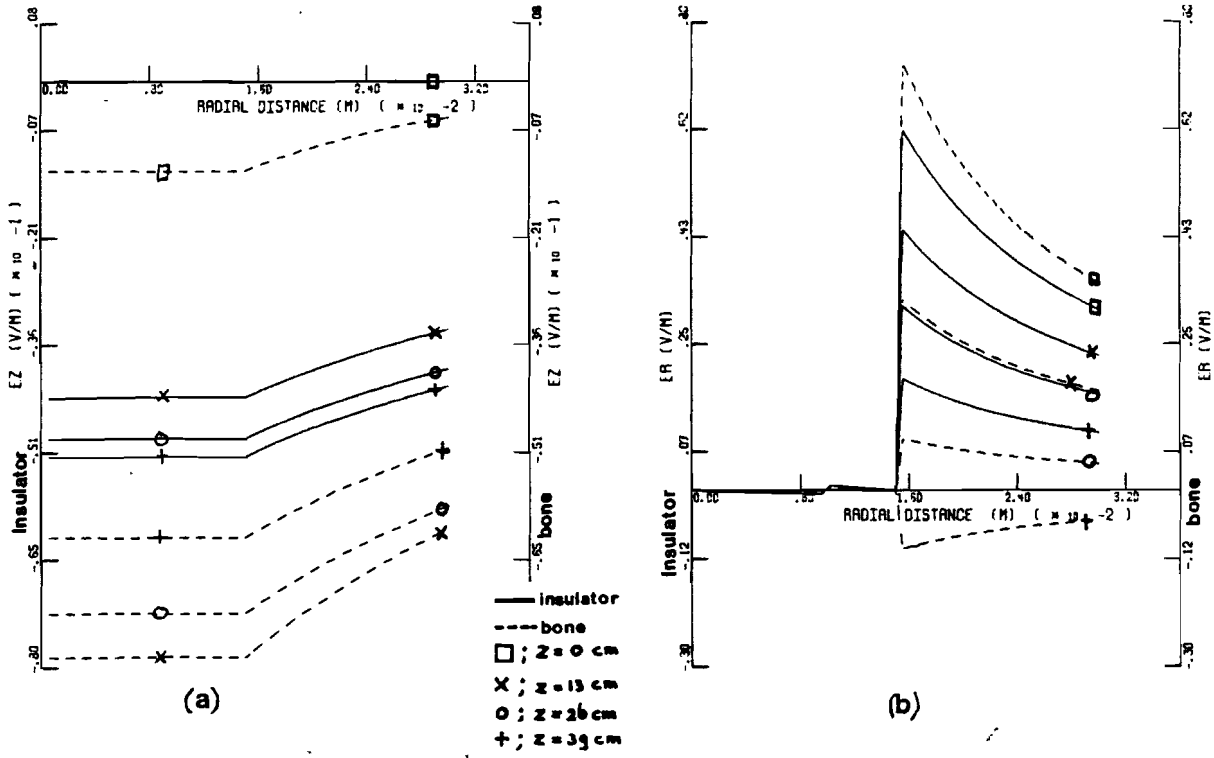

Fig.4.5 field distribution for both configurations as a function of radial distance in various transverse planes. The source frequency is f_s= 1 MHz; (a) axial field (E_z), (b) radial field (E_r)

Across the boundaries the axial field component is continuous and the radial field component is discontinuous. The axial field component is maximum in the interior region. The radial field component is almost zero in the interior region and maximum just outside this region.

The same computations have been made for both configurations excited at a source frequency f_s=1 Hz. The results are shown in Fig.4.6 and 4.7.

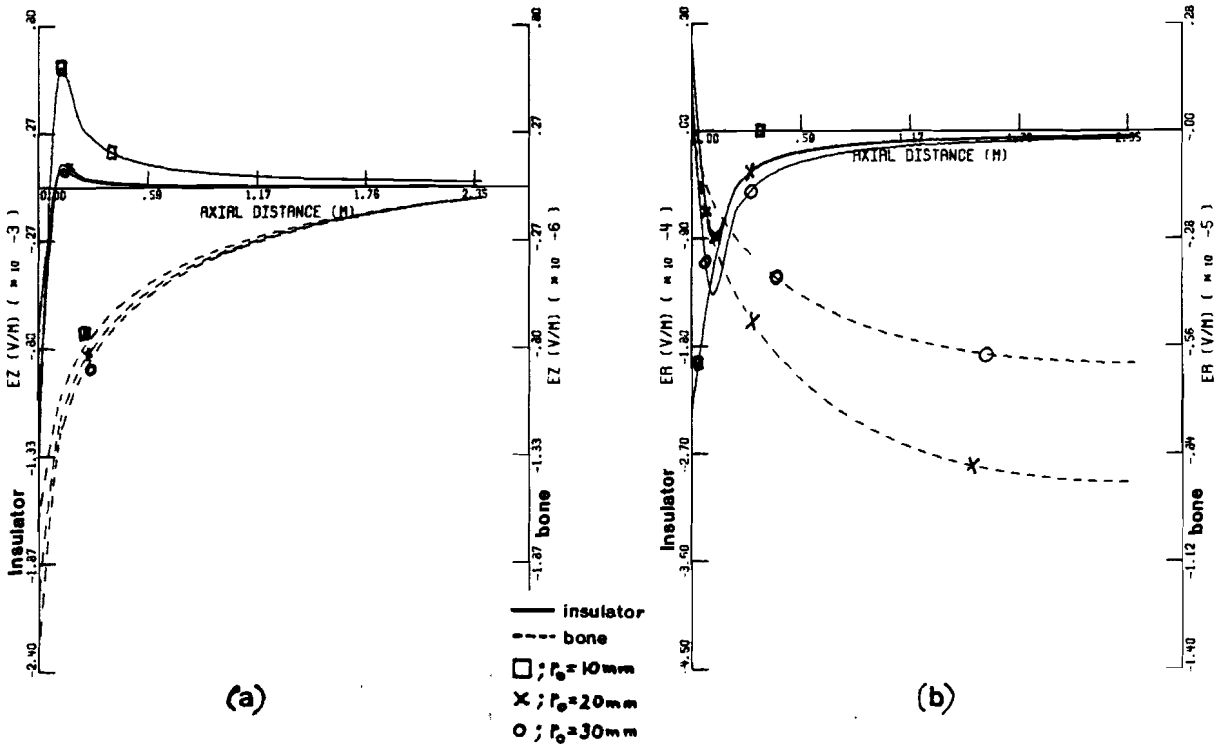

Fig.4.6 Field distribution for both configurations as a function of the axial coordinate at various radial distances. The source frequency is f_s= 1 Hz; (a) axial field (E_z), (b) radial field (E_r).

The field components are larger for the insulator configuration than for the bone configuration. The axial field component decays with increasing axial distance. The radial component first tends to get larger and, after reaching a maximum, becomes smaller when increasing axial distance to the source. Again, interchanging the roles between the axial and radial distances, Fig.4,7 shows the field components as a function of the radial distance in various transverse planes.

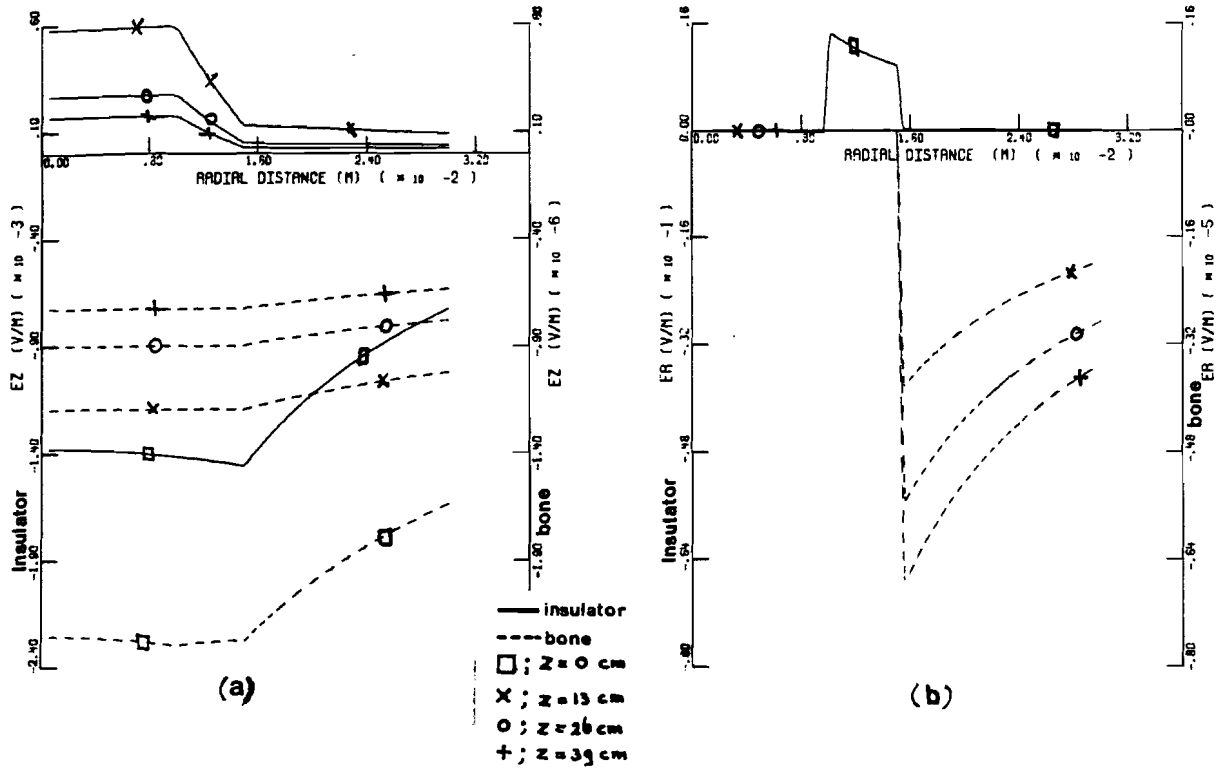

Fig.4.7 Field distribution for both configurations as a function of radial distance in various transverse planes. The source frequency is f_s= 1 Hz; (a) axial field (E_z) (b) radial field (E_r).

It can be seen that the radial component for the insulator configuration is largest in the transverse plane z=0, just between the source and the boundary which cannot be observed in the plots for the bone configuration.

Using the figures, the field pattern itself can be constructed for the 4 cases. The field patterns for the insulator and bone configurations with a source frequency f_s=1 MHz are shown in Fig.4.8.

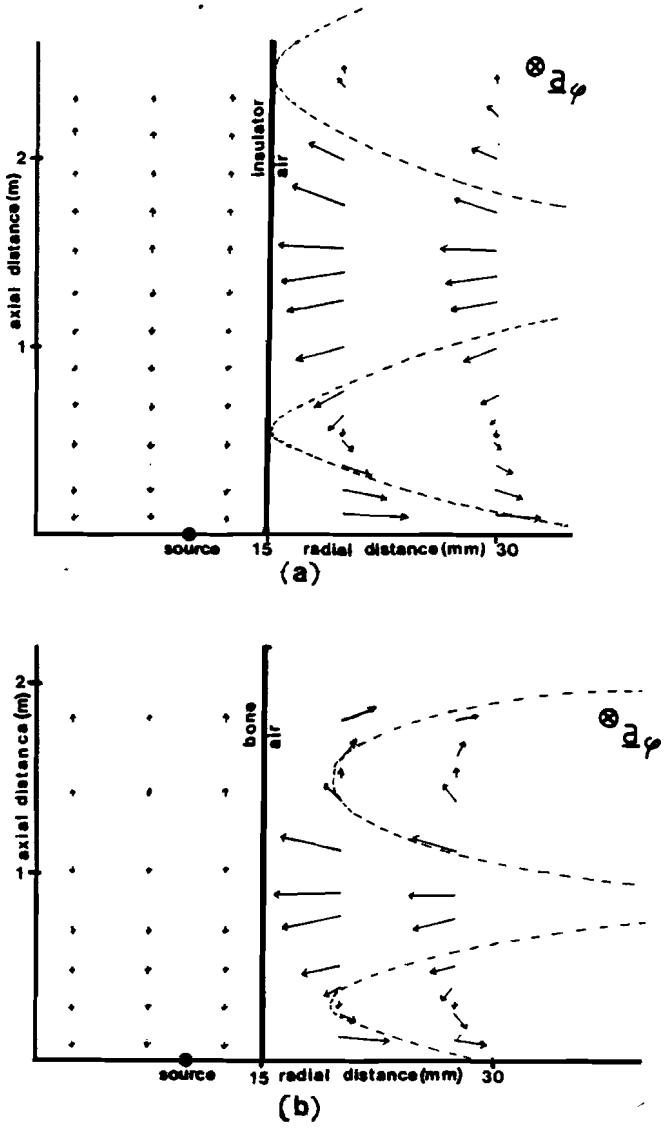

Fig.4.8 Field pattern for both configurations with a source frequency f_s= 1 MHz; (a) insulator, (b) bone

Because the construction is done by hand, only qualitative remarks are given. The drawings show the field within the central region being almost parallel to the z-axis. The field patterns for the two systems excited with a source frequency f_s=1 Hz, are given in Fig.4.9 . The typical wave distribution cannot be seen and the influence of the conductivity on the field distribution is apparent.

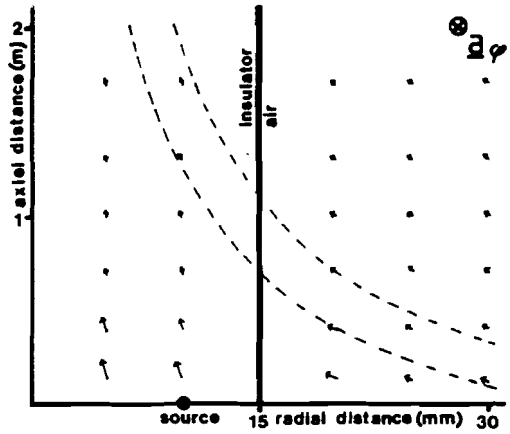

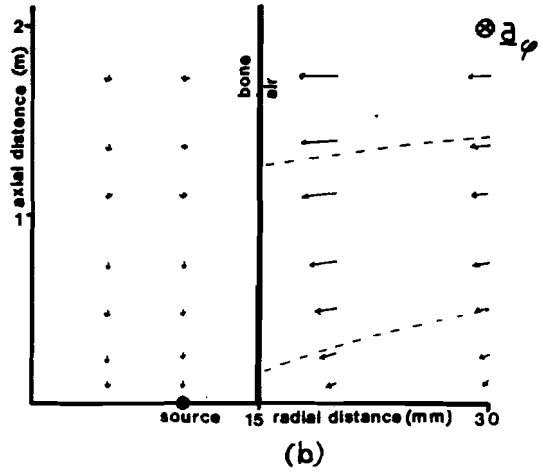

Fig.4.9 Field pattern for both configurations with a source frequency f_s= 1 Hz; (a) insulator, (b) bone

5.0 DISCUSION AND CONCLUSIONS

Some of the observations made can be explained by the fact that the different electrical properties are introducing a surface distribution of free electric charge on the boundary surface. Free charge moves with a characteristic relaxation time factor

$$\tau = \frac{\varepsilon'}{\sigma} \tag{5.1}$$

So, for low source frequences

$$f_s \ll \tau_t^{-1} \tag{5.2}$$

free charge can move almost instantaneously towards the boundary surface shielding the charged ring. But, if the source frequency is high

$$f_s \gg \tau_t^{-1} \tag{5.3}$$

the source is changing to fast for the charge to follow and retardation effects are the result. When

$$f_s \approx \tau_t^{-1} \tag{5,3}$$

both, shielding and retardation effects occur. The transverse relaxation time factors are,

$\tau_{t,2} = 8.8$ μsec , $\tau_{t,1} = 13$ μsec (bone), $\tau_{t,1} = \infty$ (insulator).

These differences in time factors, make some of the differences in the field distributions of the two configurations plausible. The interior region of the insulator configuration cannot contribute any free charge to the boundary surface ($\tau=\infty$) so, no shielding occurs at low source frequences. The field pattern for the insulator configuration excited at a source frequency f_s=1 MHz resembles the pattern of a surface wave, described by Stratton [14].

Although the computer model described in this report still needs a thorough investigation, some conclusions may be drawn

-The model is suitable for calculating the time harmonic electric field in a composite open boundary electromagnetic wave guide excited by a homogeneously charged ring source

-The anisotropy of the various layers has a great influence on the field distribution, when the source frequency $f_s \approx \tau_t^{-1}$.

-The differnt electrical properties of the various layers results in a surface charge density on the boundary surface.

-The computer model has a large dynamic range for different parameters. No numerical singularities have been observed for the following intervalls;

$$1 \text{ Hz} \leq f_s \leq 1 \text{ MHz} ,$$

$$\varepsilon_0 \leq \varepsilon' \leq 10000 \cdot \varepsilon_0 ,$$

$$0 \leq \sigma \leq 2 \cdot 10^{-2} .$$

6.0 CLINICAL ILLUSTRATION

As an illustration the method described has been used to calculate the electromagnetic field for a clinical experiment on electrical stimulated osteogenesis. Although many other clinical experiments have been done, for our purpose the experiments carried out by Janssen [8] has been choosen. The experiments where done with two intramedullary placed electrodes in a dog femur. As a first approximation the dog femur is modelled by the bone configuration described in chapt.4, the electrodes by two homogeneous charged rings, with opposite signs, placed at an axial distance of 13 cm, see Fig.6.1.

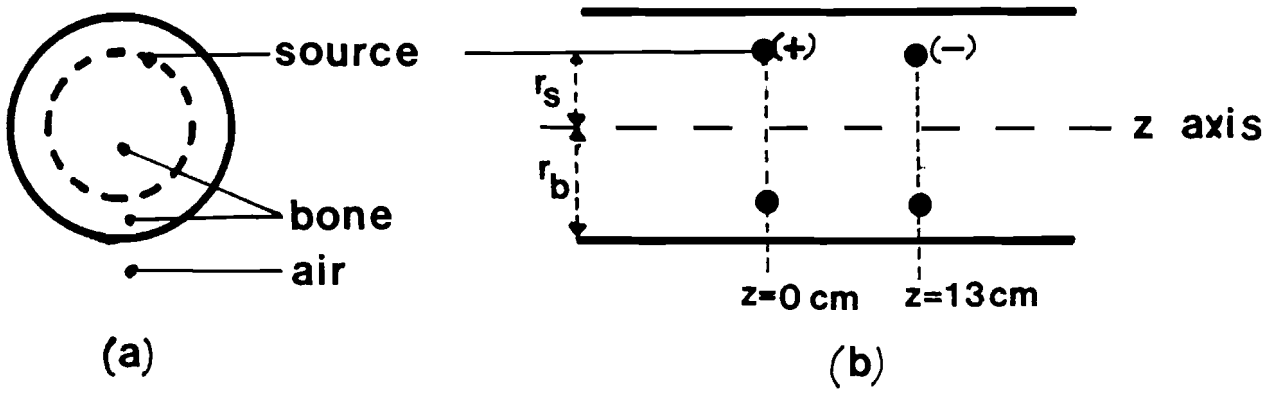

Fig.6.1 Schematic drawing of the clinical configuration;
(a) cross section,(b) longitudinal section.

In the experiments the source frequency was zero. Therefore we use the results for a quasi-static source (f_s=1 Hz). The system being linear, the responses for the charged rings can be examined separately and summed afterwards. This has been done for the axial and the radial field components and the results are shown in Fig.6.2

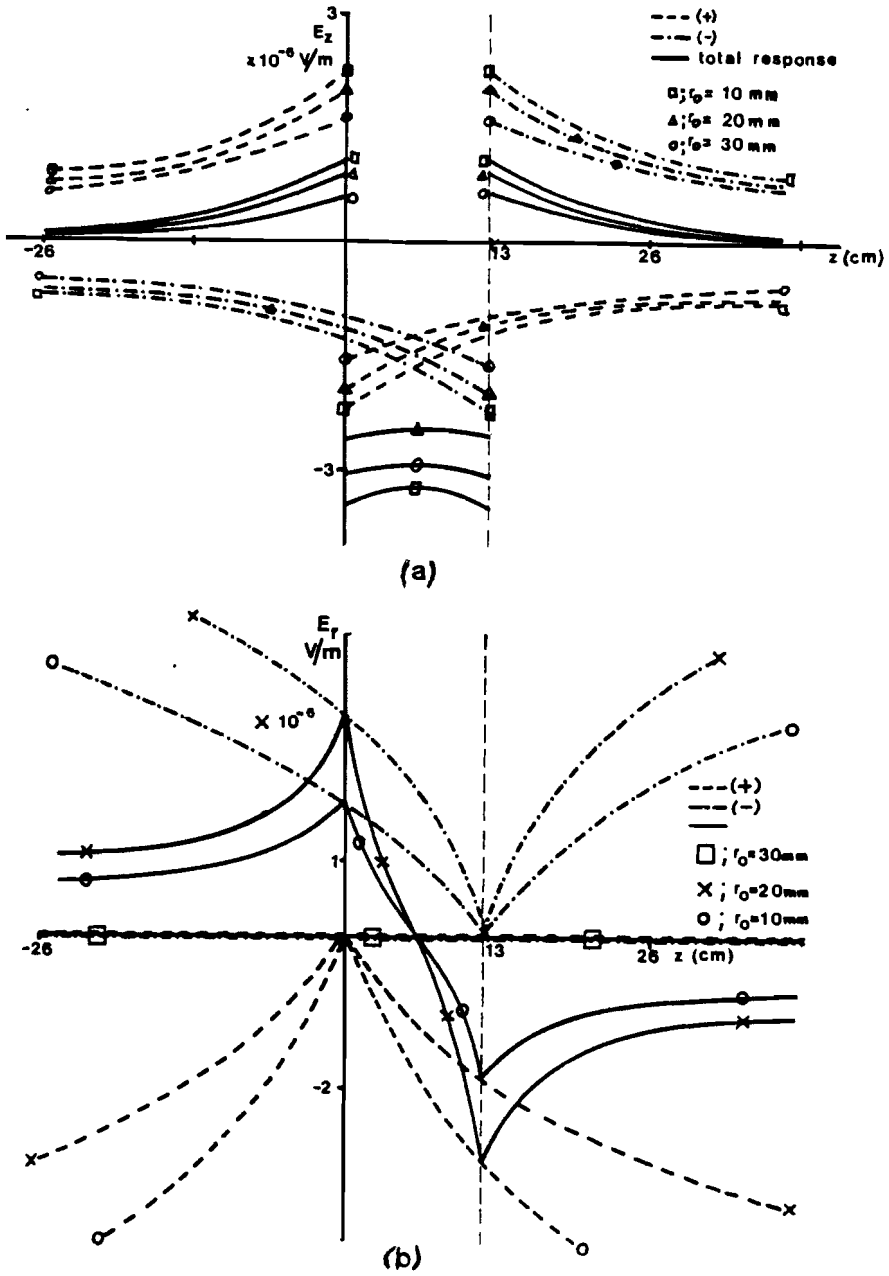

Fig.6.2 Field distribution for the clinical configuration as a function of the axial coordinate for various radial distances; (a) axial field (E_z), (b) radial field (E_r).

The field distribution is not homogeneous between the two electrodes and decay's outside this axial section. The axial component is maximum within the interior region. The radial field component is almost zero within the interior region and maximum just outside this region. Using these curves to construct the field pattern leads to the pattern shown in Fig.6.3

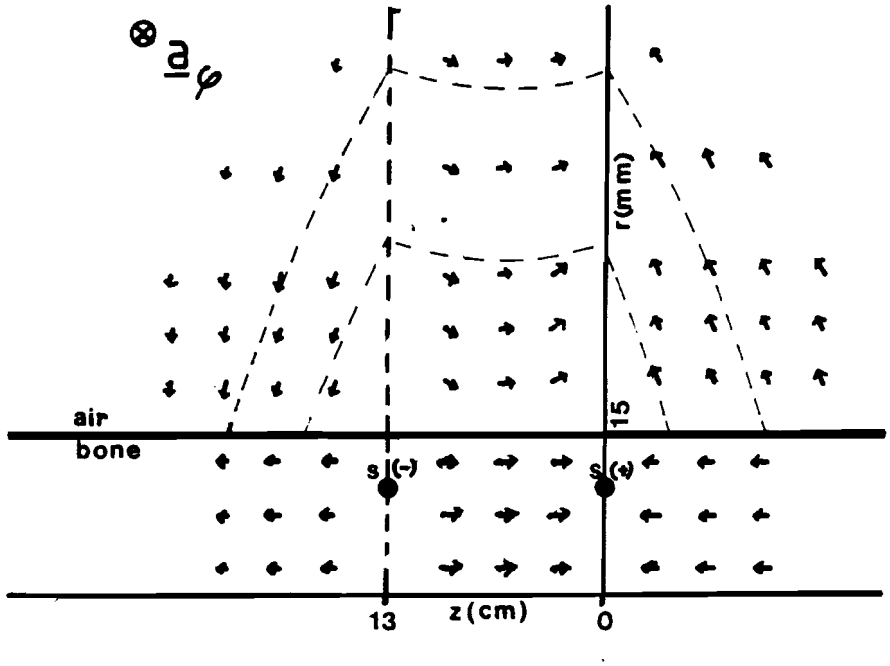

Fig.6.3 Electric field pattern for the clinical configuration excited at f_s= 1 Hz.

As can be seen, within the interior region the field is almost parallel to the z axis. Again the discontinuity in the direction can be explained by the excistance of a surface charge distribution on the boundary surface.

Although the clinical configuration does not entirely resemble the femur system, some conclusions can be drawn

-The field is inhomogeneous,

-The field decays with increasing axial distance,

-The source induces not only a charge distribution in the vicinity of the electrodes (electro chemical double layer), but also at the boundary surface.

With the results for the clinical configuration some qualitative remarks can be made about the field in the femur system itself

-The field will decay more rapidly because the introduction of marrow and muscle, which conductivities are larger than those for bone, which yields a larger power dissipation,

-The source is inducing a surface charge distribution the boundary surfaces.

The first remark indicates that the model can properly be used to calculate the electromagnetic field for an intact femur system. As a second remark we suggest that, if the induced charge is the actual stimulus, in vitro experiments on electrical stimulated osteogenesis, omitting artificial boundary surfaces would give no osteogenesis.

REFERENCES.

[1] Bassett, C.A.L., Pilla, A.A. and Pawluk, R.J.; A non-operative salvage of surgically-resistant pseudarthrosis and non-unions by pulsing electromagnetic fields; Clin. Orthop. 124,128-143(1977).

[2] Becker, R.O.; The significance of electrically stimulated osteogenesis, more questions than answers; Clin. Ortop. and rel. res. 141,266-274(1979).

[3] Brown, W.S.; ALTRAN user's manual; Murray Hill, New Jersey,(1977)

[4] Chakkalakal, D.A.,Johnson, M.W., Harper, R.A. and Katz, J.L.; Dielectric properties of fluid saturated bone; I.E.E.E. Trans. Bio. med. Eng 27(2),95-100(1980).

[5] Chakkalakal, D.A. and Johnson, M.W.; Electrical properties of compact bone; Clin. Orthop. 161,133-145(1981).

[6] Collin, R.E.; Field theory of guided waves,Mc Graw-Hill, New York,(1960).

[7] Hambrecht, F.I. and Reswick, J.B.; Functional electrical stimulation, Applications in neural prostheses, Marcel Dekker Inc.,New York, (1977).

[8] Janssen, L.W.M.; Electrical stimulation of bone tissue, a clinical and experimental study, thesis, Utrecht University Hospital (The Netherlands), (1978).

[9] Oppenheim, A.V. and Schafer, R.W.; Digital signal processing, Prentice Hall Inc, Englewood Cliffs, New Jersey, (1975).

[10] Roberts, D.E., Scher, A.M., Effect of tissue anisotropy on extracellular potential fields in canine myocardium in situ, Circ. Res. 50, 342-351(1982).

[11] Scharten, Th.; Electromagnetisch veld II, lecture notes, Eindhoven University of Technology (The Netherlands), 5.523 (1980).

[12] Scharten,Th.; Using boundary equations in guided wave problems, with application to uniform rectangular structures (to be published)

[13] Spadaro, J.A.; Bioelectric stimulation of bone formation, methods, models and mechanisms, J. Bioelectricity, 1(1),99-128 (1982).

[14] Stratton, J.A.; Electromagnetic theory, Mc Graw-Hill, New York, (1941).

[15] Vaughan, J.M.; The physiology of bone, Oxford, Clarendon Press, (1970).

[16] Yasuda, I.; Fundamental aspects of fracture treatment, Clin. Orthop. 124,5-8 (1977).

APPENDIX A

Algorithm

It has been shown that in each layer, the transformed Green functions can be written as a linear combinations of Bessel and Neumann function

$$E_{z,i} = C^{e}_{J,i} J_n(\kappa^{e} r) + C^{e}_{Y,i} Y_n(\kappa^{e} r) \qquad r_{i-1} < r < r_i \quad \text{(A.1a)}$$

$$H_{z,i} = C^{h}_{J,i} J_n(\kappa^{h} r) + C^{h}_{Y,i} Y_n(\kappa^{h} r). \qquad r_{i-1} < r < r_i \quad \text{(A.1b)}$$

In the following an algorithm will be derived, to find the coefficients as a function of the source strength, for an arbitrary number of layers and an arbitrary source location. Only the primary electric current density acts as the source ($\underline{K}=\underline{0}$) and furthermore, it is assumed that $\mu_t = \mu_z = \mu_0$.

First the various layers and boundaries are re-numbered, to include the source as an extra boundary at $r=r_s$. After imaginairy splitting up the layer containing the source, the layers are re-numbered, starting with 1 for the interior region and then incrementing to the exterior region. The same is done with the boundaries, where r_i $(i=s)=r_s$, see Fig.A.1.

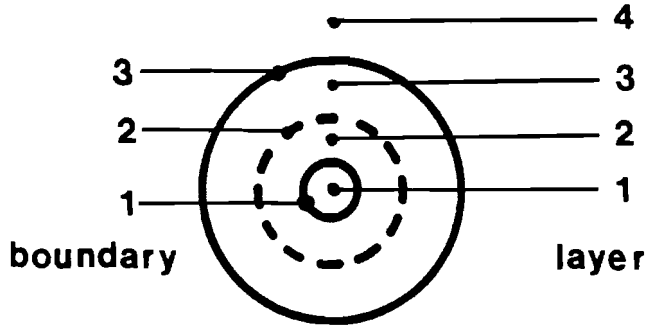

Fig.A.1 The re-numbering of the layers and boundaries.

In total, there are 4×(N+1) coefficients to determine, by as many boundary conditions; 4×(N-1) times

$$E_z^- = E_z^+ \qquad r=r_i,\ r\neq r_s \qquad \text{(A.2a)}$$

$$E_\phi^- = E_\phi^+ \qquad r=r_i,\ r\neq r_s \qquad \text{(A.2b)}$$

$$H_z^- = H_z^+ \qquad r=r_i,\ r\neq r_s \qquad \text{(A.2c)}$$

$$H_\phi^- = H_\phi^+ \qquad r=r_i,\ r\neq r_s \qquad \text{(A.2d)}$$

and 4 at the source location,

$$E_z^- = E_z^+ \qquad r=r_s \qquad \text{(A.3a)}$$

$$\partial_r E_z^- = \partial_r E_z^+ - \frac{j\beta\rho}{\varepsilon_t r_s} \qquad r=r_s \qquad \text{(A.3b)}$$

$$H_z^- = H_z^+ \qquad r=r_s \qquad \text{(A.3c)}$$

$$\partial_r H_z^- = \partial_r H_z^+ \qquad r=r_s \qquad \text{(A.3d)}$$

the solution being bounded results in two conditions at the origin,

$$E_{z,1} = C^e_{J,1} J_n(\kappa^e r) \qquad r<r_1 \qquad \text{(A.4a)}$$

$$H_{z,1} = C^h_{J,1} J_n(\kappa^h r) \qquad r<r_1 \qquad \text{(A.4b)}$$

and another 2 for $r \to \infty$,

$$E_{z,N+1}=C^{e}_{J,N+1}(J_n(\kappa^{e}r) - jY_n(\kappa^{e}r)) \qquad r>r_N \qquad (A.4c)$$

$$H_{z,N+1}=C^{h}_{J,N+1}(J_n(\kappa^{h}r) - jY_n(\kappa^{h}r)) \qquad r>r_N \qquad (A.4d)$$

Using matrix algebra the equations at the boundaries can be written as ($1 \leq i \leq N$)

$$\underline{\underline{A}}_i \cdot \underline{C}_i = \underline{\underline{B}}_i \cdot \underline{C}_{i+1} \qquad r=r_i,\ r \neq r_s \qquad (A.5a)$$

$$\underline{C}_i=\underline{C}_{i+1}+\underline{\underline{D}}^{-1} \cdot \underline{S} \qquad r=r_s \qquad (A.5b)$$

where

$$\underline{C}_i=(C^{e}_{J,i},C^{e}_{Y,i},C^{h}_{J,i},C^{h}_{Y,i})^{T} \qquad (A.6a)$$

$$\underline{C}_{i+1}=(C^{e}_{J,i+1},C^{e}_{Y,i+1},C^{h}_{J,i+1},C^{h}_{Y,i+1})^{T} \qquad (A.6b)$$

and

$$\underline{\underline{A}}_i = \begin{bmatrix} J_n(\kappa^{e}_i r_i) & Y_n(\kappa^{e}_i r_i) & 0 & 0 \\ 0 & 0 & J_n(\kappa^{h}_i r_i) & Y_n(\kappa^{h}_i r_i) \\ p\ J_n(\kappa^{e}_i r_i) & p\ Y_n(\kappa^{e}_i r_i) & q\ J'_n(\kappa^{h}_i r_i) & q\ Y'_n(\kappa^{h}_i r_i) \\ s\ J'_n(\kappa^{e}_i r_i) & s\ Y'_n(\kappa^{e}_i r_i) & p\ J_n(\kappa^{h}_i r_i) & p\ Y_n(\kappa^{h}_i r_i) \end{bmatrix} \qquad (A.7a)$$

$$\underline{\underline{B}}_i = \begin{bmatrix} J_n(\kappa^e_{i+1} r_i) & Y_n(\kappa^e_{i+1} r_i) & 0 & 0 \\ 0 & 0 & J_n(\kappa^h_{i+1} r_i) & Y_n(\kappa^h_{i+1} r_i) \\ 0 & 0 & t\, J'_n(\kappa^h_{i+1} r_i) & t\, Y'_n(\kappa^h_{i+1} r_i) \\ v\, J'_n(\kappa^e_{i+1} r_i) & v\, Y'_n(\kappa^e_{i+1} r_i) & 0 & 0 \end{bmatrix} \tag{A.7b}$$

$$\underline{\underline{D}} = \begin{bmatrix} J_n(\kappa^e_s r_s) & Y_n(\kappa^e_s r_s) & 0 & 0 \\ 0 & 0 & J_n(\kappa^h_s r_s) & Y_n(\kappa^h_s r_s) \\ \kappa^e_s J'_n(\kappa^e_s r_s) & \kappa^e_s Y'_n(\kappa^e_s r_s) & 0 & 0 \\ 0 & 0 & \kappa^h_s J'_n(\kappa^h_s r_s) & \kappa^h_s Y'_n(\kappa^h_s r_s) \end{bmatrix} \tag{A.7c}$$

where

$$p = \omega\, j\beta\, r_i^{-1} n\, \mu\, (\varepsilon_{t,i+1} - \varepsilon_{t,i}) \tag{A.7d}$$

$$q = \mu\, \kappa^2_{i+1} \kappa^h_i \tag{A.7e}$$

$$s = -\, \varepsilon_{t,i} \kappa^2_{i+1} \kappa^e_i \tag{A.7f}$$

$$t = \mu\, \kappa_i^2 \kappa^h_{i+1} \tag{A.7g}$$

$$v = -\, \varepsilon_{t,i+1} \kappa_i^2 \kappa^e_{i+1} \tag{A.7h}$$

and the source vector

$$\underline{S} = (0, \quad 0 \ , -\frac{j\beta\ \rho}{\varepsilon_t r_s} \ , \ 0 \ )^T. \qquad \text{(A.7i)}$$

The prime in the Bessel and Neumann functions denotes differentiation with respect to κr.

With matrix multiplications, it can be shown that

$$\underline{C}_j = \Big[\prod_{i=j-1}^{1} (\underline{\underline{B}}_i^{-1} \cdot \underline{\underline{A}}_i) \Big] \cdot \underline{C}_1 \qquad j < s \qquad \text{(A.8)}$$

and

$$\underline{C}_j = \Big[\prod_{i=j}^{N} (\underline{\underline{A}}_i^{-1} \cdot \underline{\underline{B}}_i) \Big] \cdot \underline{C}_{N+1} . \qquad j > s \qquad \text{(A.9)}$$

The coefficients of layer 1 can now be expressed as a function of those of the exterior layer and the source vector

$$\Big[\prod_{i=s-1}^{1} (\underline{\underline{B}}_i^{-1} \cdot \underline{\underline{A}}_i) \Big] \cdot \underline{C}_1 = \Big[\prod_{i=s+1}^{N} (\underline{\underline{A}}_i^{-1} \cdot \underline{\underline{B}}_i) \Big] \cdot \underline{C}_{N+1} + \underline{\underline{D}}^{-1} \cdot \underline{S} \qquad \text{(A.10)}$$

or,

$$\Big[\prod_{\substack{i=N \\ i \neq s}}^{1} (\underline{\underline{B}}_i^{-1} \cdot \underline{\underline{A}}_i) \Big] \cdot \underline{C}_1 = \underline{C}_{N+1} + \Big[\prod_{i=N}^{s+1} (\underline{\underline{B}}_i^{-1} \cdot \underline{\underline{A}}_i) \Big] \cdot \underline{\underline{D}}^{-1} \cdot \underline{S} \qquad \text{(A.11)}$$

Using eqns.(A.4) 4 coefficients can be eliminated and, after defining

$$\Big[\prod_{\substack{i=N \\ i \neq s}}^{1} (\underline{\underline{B}}_i^{-1} \cdot \underline{\underline{A}}_i) \Big] = \begin{bmatrix} a_{1,1} & a_{1,2} & a_{1,3} & a_{1,4} \\ a_{2,1} & a_{2,2} & a_{2,3} & a_{2,4} \\ a_{3,1} & a_{3,2} & a_{3,3} & a_{3,4} \\ a_{4,1} & a_{4,2} & a_{4,3} & a_{4,4} \end{bmatrix} \qquad \text{(A.12)}$$

the 4 coefficients left can be determined by

$$(C^{e}_{J,1}, C^{h}_{J,1}, C^{e}_{J,N+1}, C^{h}_{J,N+1})^{T} = \underline{\underline{DSP}}^{-1} \cdot \left[\prod_{i=N}^{s+1} (\underline{\underline{B}}_{i}^{-1} \cdot \underline{\underline{A}}_{i}) \right] \cdot \underline{S} \qquad (A.13)$$

where the dispersion matrix ($\underline{\underline{DSP}}$) is defined by

$$\underline{\underline{DSP}} = \begin{bmatrix} a_{1,1} & a_{1,3} & -1 & 0 \\ a_{2,1} & a_{2,3} & j & 0 \\ a_{3,1} & a_{3,3} & 0 & -1 \\ a_{4,1} & a_{4,3} & 0 & j \end{bmatrix} \qquad (A.14)$$

Finally the coefficients of the inner and outer layers are expressed as an explicit function of the source. The other coëfficients can then be determined by using the same matrices as in eqns.(A.8) and eqns.(A.9)

So far, no numerical values have been assigned to one of the parameters involved. Furthermore, as the coefficients could be expressed as an explicit function of the parameters, the results could be applied to different circular cilindrical waveguides (glass fiber). Although it is not practical to write out the algorithm by hand, the algorithm can be used to find the coefficients with the help of a computer with a program-language that can manipulate algebraic forms. Such a language is ALTRAN [3], blockdiagrams of the programs used for the algorithm as well as the numerical analysis are given in appendix B.

APPENDIX B

The algorithms derived in this report have been used to write a computer program which could determine the electromagnetic field distribution. Before a numerical computation can be made (in FORTRAN) the formulae for the coeficients are derived using a programming language called ALTRAN. In this appendix the block diagrams are given for both programs, first that for ALTRAN procedures, secondly for FORTRAN procedures.

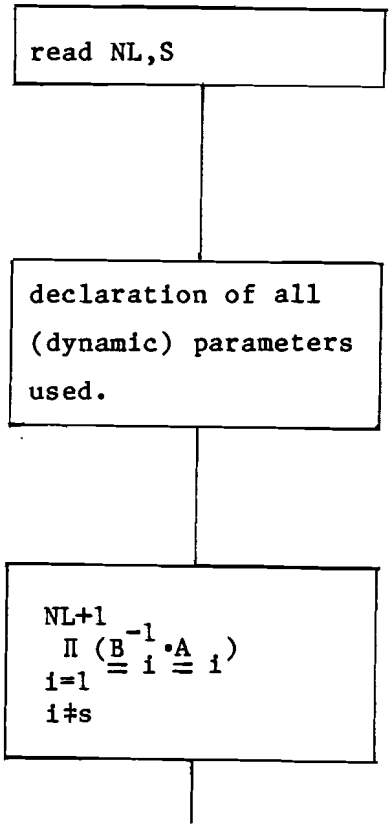

First the number of layers (NL) the system consist of, and the layer containing the source (S) are read.

Because the number of parameters depend on the number of layers, the indeterminates are declared dynamic, and therefor needs to be initiated.

The different matrix multiplications are performed to find the dispersion matrix ($\underline{\underline{DSP}}$).

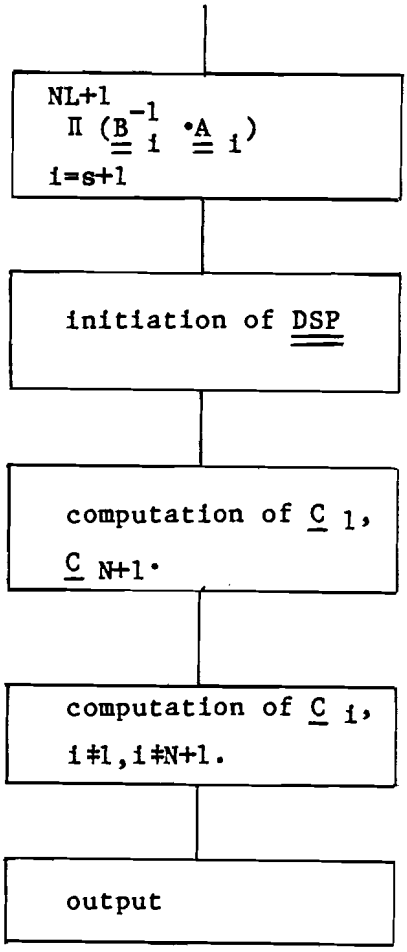

The coefficients of the inner and outer regions are computed.

The coefficients of the other layers are expressed as a function of the parameters.

The coefficients are written on a file for further use.

The file containing the forms for the coefficients are then translated to correct FORTRAN statements and inserted into the FORTRAN program.

The FORTRAN program to calculate the numerical value of the field distributions has the following structure.

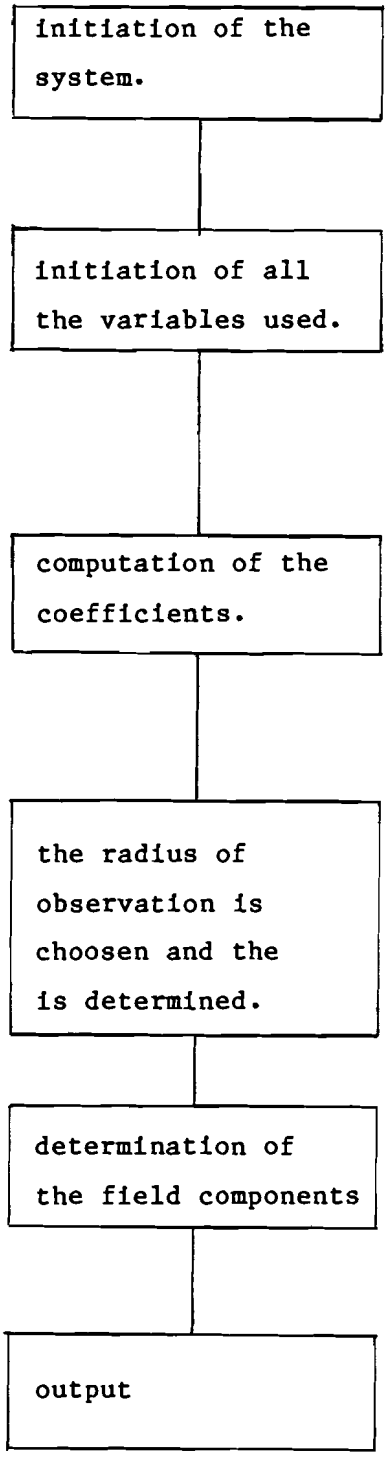

The system will be defined. Numerical values are assigned to all the parameters involved.

The dielectric constants (ε) and wave numbers (κ) obtain their complex values and the Bessel and Neumann functions are computed for the various arguments.

Complex numerical values are assigned to the coefficients using the formula obtained form the ALTRAN program.

Because each layer has it's own set of coefficients, the layer in which the the observator is located must be determined before the field distribution

Finally the field components are computed using the appropriate coefficients and the Bessel and Neumann functions.

The output depends largely on the wishes of the user. A choice can be made between the amplitude spectra or one of the field distributions for various radial distances or source frequences.